# α-Diimine, Diamine, and Diphosphine Iron Catalysts for the Controlled Radical Polymerization of Styrene and Acrylate Monomers

**Rachel K. O'Reilly, Michael P. Shaver, Vernon C. Gibson,* and Andrew J. P. White**

*Department of Chemistry, Imperial College, Exhibition Road, South Kensington, London, SW7 2AZ, U.K.*

*Received March 29, 2007; Revised Manuscript Received July 5, 2007*

ABSTRACT: The synthesis and characterization of a family of iron complexes of the type $^{R}[N,N]FeX_2$ ($X$ = halide; $^{R}[N,N]$ = RN═CH−CH═NR, R = alkyl, aryl) and their application as catalysts for the controlled polymerization of styrenyl and acrylate monomers is described. Polymerizations catalyzed by alkylimine iron complexes give rise to atom transfer radical polymerization (ATRP) of styrene and methyl methacrylate, while those catalyzed by arylimine iron complexes give rise to catalytic chain transfer polymerization. A study of the ketimine series, $^{R,Me}[N,N]FeCl_2$ (where $^{R,Me}[N,N]$ = RN═C(Me)−C(Me)═NR, R = Cy, Ph, DiPP), showed that electronic factors govern the mechanistic pathway. Controlled polymerizations were also observed for methyl acrylate and *p*-methoxystyrene monomers. Moderate control over the polymerization of 2-hydroxypropyl methacrylate was achieved in methanolic solution using methyl-α-bromophenylacetate as an initiator. The analogous diamine and diphosphine iron complexes, $(Et_2NCH_2CH_2NEt_2)FeCl_2$ and $(R_2PCH_2CH_2PR_2)FeCl_2$ (R = *i*-Pr, Ph, $C_6F_5$, $C_6H_{11}$, Et), were also prepared and screened for ATRP behavior. The phosphine complexes were found to be the most reducing in the series, followed by the amines and then the imines, but large peak-to-peak ($\Delta E_p$) separations, indicative of poor reversibility, resulted in their poor performance as ATRP catalysts.

## Introduction

Atom transfer radical polymerization (ATRP) has become established as a versatile technique for the synthesis of a wide range of materials derived from styrene, methacrylate and acrylate monomers.[1,2] Building on the known use of metals to catalyze the coupling of organic radicals (the Kharasch reaction), Matyjaszewski[3] and Sawamoto[4] introduced copper- and ruthenium-based systems capable of mediating the atom transfer radical polymerization reaction (eqs 1 and 2). Key to the success of metal complexes in the polymerization process is a readily accessible and reversible redox couple. Furthermore, a low concentration of radicals must be maintained in order to avoid undesirable chain termination reactions involving the coupling of radical centers.

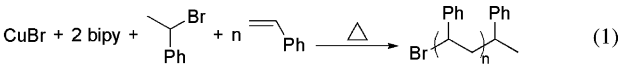

(1)

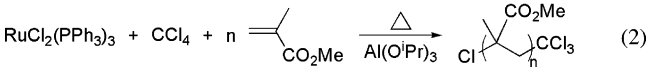

(2)

The copper-based systems have been elaborated extensively using a range of ancillary ligands including pyridylimines,[5−7] bi- and multidentate amines,[8−11] bis(imino)pyridines,[12] and a number of other nitrogen donor combinations.[13−17] Sawamoto and co-workers extended the Group 8 metal systems to iron analogues of their ruthenium catalyst and found that an activator was no longer required for the efficient polymerization of methyl methacrylate (MMA).[18] Examples of iron and ruthenium based ATRP catalysts bearing carbon centered ligands such as cyclopentadienyl and indenyl have also been reported.[19−21] These complexes were found to be more active than the phosphine complexes and have been used to polymerize styrene, MMA and acrylates.[22,23] Matyjaszewski and co-workers have reported several iron based ATRP systems based on iron(II) bromide in combination with phosphino and amino ligands[24] and also phosphonium and ammonium halides.[25]

Our interest in ATRP grew out of our investigations into iron-based olefin polymerization catalysts.[26] In exploring [bis(imino)-pyridine]$FeCl_2$ systems as precatalysts for ethylene polymerization it was noticed that their redox properties should be ideally suited to ATRP. Subsequent studies showed that these catalysts do indeed mediate ATRP, but a disappointing level of control was achieved.[12,27−29] For these systems it seems likely that steric crowding around the iron center may disfavor formation of the oxidized six-coordinate [bis(imino)pyridine]$FeCl_3$ complex. This led us to focus our attention on systems operating via the interconversion of four- and five-coordinate species. It was anticipated that the more open coordination sphere of a four-coordinate $Fe^{II}$ complex would allow more ready accommodation of a halogen atom, while the greater geometrical flexibility of the oxidized five-coordinate species, for example via pseudo-rotation, might allow the catalyst to access a coordination geometry more suited to dissociative loss of a halogen atom.

The use of α-diimine iron complexes for the controlled polymerization of styrene has been reported by our group in preliminary communications.[30,31] Polymerizations catalyzed by arylimine stabilized iron catalysts gave rise to the catalytic chain transfer polymerization of styrene, while those catalyzed by alkylimine derivatives afforded ATRP behavior. Further work has since correlated the prevalence of ATRP vs CCT mechanisms to the spin state of the iron(III) complex, showing that modification of the 2- and 3-positions on the diimine backbone affords control over the metal spin-state and the polymerization mechanism.[32,33] In a separate study, we have also investigated the role of organometallic intermediates in the chain transfer process.[34]A recent review has examined the interplay of ATRP, organometallic mediated radical polymerization (OMRP) and CCT processes.[35]

* Corresponding author. Fax: 020 7594 5810; Telephone: 020 7594 5830. E-mail: v.gibson@imperial.ac.uk.

10.1021/ma070756j CCC: $37.00 © 2007 American Chemical Society
Published on Web 09/14/2007

**Scheme 1. Synthesis of Complexes 1−13**

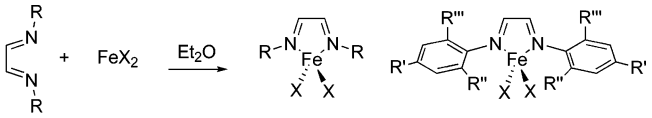

| X = Cl | | X = Cl | | X = Br | |
|---|---|---|---|---|---|
| R = $^t$Bu | **1** | R′ = R″ = R‴ = Me | **7** | R = $^t$Bu | **11** |
| R = Cy | **2** | R′ = H, R″ = R‴ = $^i$Pr | **8** | R = Cy | **12** |
| R = *c*-$C_{12}H_{23}$ | **3** | R′ = R″ = H, R‴ = Me | **9** | R′ = H, R″ = R‴ = $^i$Pr | **13** |
| R = Adamantyl | **4** | R′ = Br, R″ = R‴ = Me | **10** | | |
| R = $^i$Pr | **5** | | | | |
| R = $^i$Bu | **6** | | | | |

Herein we describe the synthesis and characterization of an extended family of $^R$[*N*,*N*]$FeX_2$ complexes, where X = Cl or Br and $^R$[*N*,*N*] is an *N*,*N*-disubstituted α-diimine ligand, an evaluation of their use as catalysts for the polymerization of styrenyl, methacrylate and acrylate monomers in bulk, hydrocarbon, and protic media, along with structural and electrochemical studies to provide insight into the factors important for the design of iron-based catalysts for controlled radical polymerization. The study is then extended to four-coordinate complexes containing diamine and diphosphine ligands to enable a comparison of imine, amine and phosphine donor functionalities in this catalyst system.

## Results

**$^R$[*N*,*N*]$FeX_2$: Synthesis and Structural Characterization.** α-Diimines are excellent ligands for four-coordinate iron ATRP catalysts due to their ease of preparation and their amenability to modification. They are readily prepared in high yield from the condensation of 2 equiv of the appropriate amine or aniline with 1 equiv of glyoxal.[36,37] Complexes **1**−**13** were synthesized using a modification of the preparation described by Dieck,[38] involving treatment of $FeCl_2$ and $FeBr_2$ with the appropriate α-diimine in diethyl ether (Scheme 1). The complexes have been characterized by microanalysis, FAB mass spectrometry, magnetic susceptibility measurements, cyclic voltammetry, and $^1$H NMR spectroscopy.

Since the key step in ATRP involves a fast and reversible halogen atom exchange between the metal center and the polymer chain-end, the coordination environment imposed by the ligand is a key factor influencing this process. We thus sought to establish the solid-state structures of a selection of complexes as a starting point for understanding their performance as ATRP catalysts; the structures of **2** and **8** have been reported previously.[30,31] Crystals of **3**, **5**, **7**, and **11** suitable for X-ray structural determination were grown from acetonitrile (**3**), from layered dichloromethane-pentane (1:1) solutions (**5**, **7**), or from a concentrated toluene solution (**11**); their structures are shown in Figures 1−4.

Complex **3** (Figure 1) possesses crystallographic $C_2$ symmetry about an axis passing through the metal center and the middle of the C(1)−C(1′) bond. The cyclododecane rings are disordered and two discrete overlapping conformations were observed. The geometry at the metal center and within the five-membered chelate ring does not differ significantly from that observed in the previously reported dicyclohexyl analogue.[30] The angles at iron are in the range 78.5(3) to 121.7(2)°, the chelate ring is planar to within 0.008 Å, and the C═N bonds exhibit pronounced double bond character [1.276(8) Å]; there is also a ca. 5° twist of the $FeCl_2$ plane with respect to the $FeN_2$ plane about the $C_2$ axis.

Contrastingly, a solid-state structure determination of **5** revealed the centrosymmetric dimer complex shown in Figure

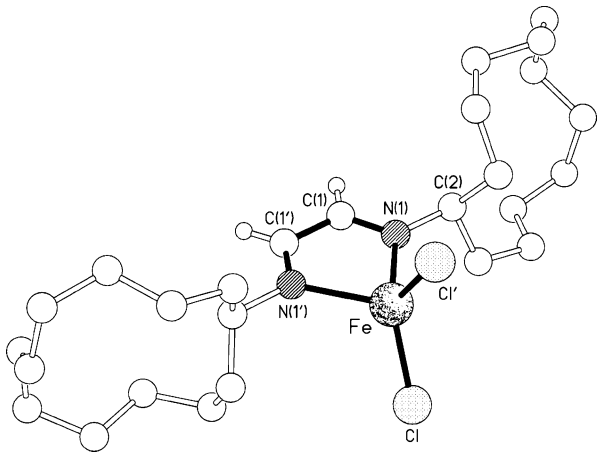


**Figure 1.** Molecular structure of the $C_2$-symmetric complex **3** (atoms with a prime suffix are related to those without the prime by the $C_2$ axis). Selected bond lengths (Å) and angles (deg): Fe−Cl, 2.217(3); Fe−N(1), 2.129(5); N(1)−C(1), 1.276(8); C(1)−C(1′), 1.467(13); N(1)−Fe−N(1′), 78.5(3); N(1)−Fe−Cl′, 109.0(2); N(1)−Fe−Cl, 115.3(2); Cl′−Fe−Cl, 121.7(2).

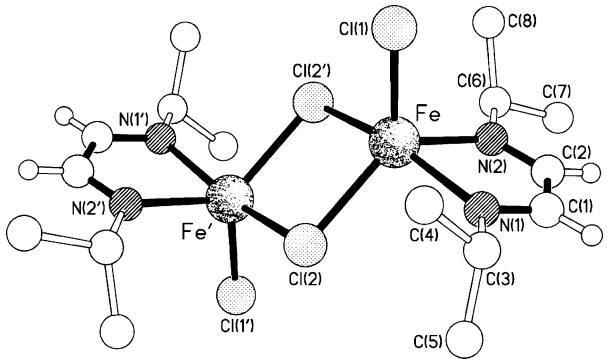


**Figure 2.** Molecular structure of the $C_i$-symmetric complex **5** (atoms with a prime suffix are related to those without the prime by the center of symmetry). Selected bond lengths (Å) and angles (deg); Fe−Cl(1), 2.2824(13); Fe−Cl(2), 2.3946(12); Fe−Cl(2′), 2.5516(12); Fe−N(1), 2.208(4); Fe−N(2), 2.152(3); N(1)−C(1), 1.273(7); C(1)−C(2), 1.464-(7); N(2)−C(2), 1.257(6); N(2)−Fe−N(1), 76.61(15); N(2)−Fe−Cl-(1), 106.92(10); N(1)−Fe−Cl(1), 97.87(10); N(2)−Fe−Cl(2), 125.59-(10); N(1)−Fe−Cl(2), 91.48(11); Cl(1)−Fe−Cl(2), 127.38(6); N(2)−Fe−Cl(2′), 93.46(10); N(1)−Fe−Cl(2′), 161.92(10); Cl(1)−Fe−Cl(2′), 99.49(5); Cl(2)−Fe−Cl(2′), 81.99(4); Fe−Cl(2)−Fe′, 98.01(4). The transannular Fe···Fe′ separation is 3.7346(12) Å.

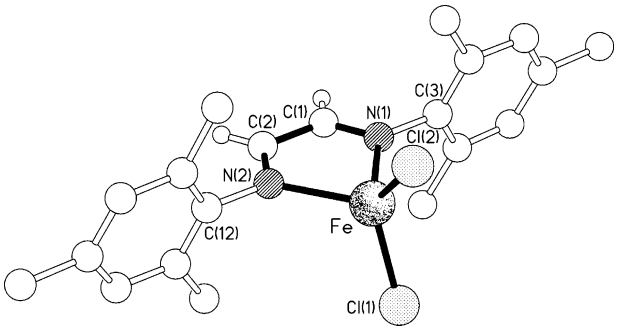


**Figure 3.** Molecular structure of **7**. Selected bond lengths (Å) and angles (deg); Fe−Cl(1) 2.228(3), Fe−Cl(2) 2.232(4), Fe−N(1) 2.098(8), Fe−N(2) 2.132(8), C(1)−N(1) 1.269(13), C(2)−N(2) 1.278(13), C(1)−C(2) 1.487(14), N(1)−Fe−N(2) 78.1(3), N(1)−Fe−Cl(1) 108.7(2), N(2)−Fe−Cl(1) 109.8(2), N(1)−Fe−Cl(2) 116.7(2), N(2)−Fe−Cl(2) 116.3(2), Cl(1)−Fe−Cl(2) 119.82(14).

2. The geometry at iron is distorted trigonal bipyramidal with N(1) and Cl(2′) occupying the axial positions [N(1)−Fe−Cl(2′) 161.92(10)°]. Within the equatorial plane the Cl(1)−Fe−Cl(2) and Cl(2)−Fe−N(2) angles are noticeably enlarged [127.38(6)

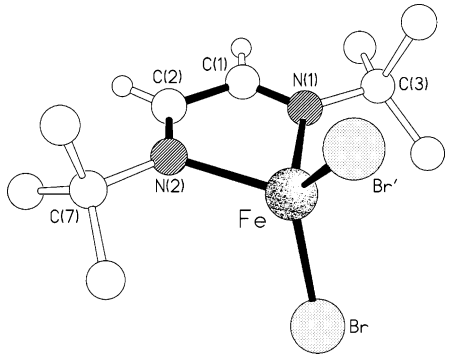


**Figure 4.** Molecular structure of **11**. Selected bond lengths (Å) and angles (deg); Fe−Br, 2.3670(13); Fe−N(1), 2.118(8); Fe−N(2), 2.105(8); C(1)−N(1), 1.219(13); C(2)−N(2), 1.230(13); C(1)−C(2), 1.467(15); N(1)−Fe−N(2), 78.8(3); N(1)−Fe−Br, 113.07(9); N(2)−Fe−Br, 113.44(9); Br−Fe−Br′, 118.53(8).

and 125.59(10)° respectively] with a consequent contraction of the Cl(1)−Fe−N(2) angle [106.92(10)°], the metal lying only ca. 0.044 Å out of the {Cl(1),Cl(2),N(2)} plane. The axial/equatorial bite of the chelating ligand shows the expected substantial contraction [N(1)−Fe−N(2) 76.61(15)°], with the five-membered chelate ring being coplanar to within 0.017 Å. The iron coordination distances are unexceptional, the axial bonds being as expected longer than their equatorial counterparts; the chloride bridges are thus asymmetric [Fe−Cl(2) 2.3946(12), Fe−Cl(2′) 2.5516(12) Å].

A single-crystal X-ray structure of the mesityl derivative, **7** (Figure 3), revealed approximate $C_S$ symmetry (cf. $C_2$ in **3**) across a plane including the metal center and the two chlorine atoms. There are marked departures from molecular $C_{2v}$ symmetry, notably ca. 7° rotations (in the same sense) from an orthogonal relationship of the planes of the mesityl rings with respect to the chelate ring plane (which is planar to within 0.040 Å). These rotations are accompanied by an axial/equatorial disposition of the two Fe−Cl bonds, the bisector of the $FeCl_2$ angle being inclined by ca. 7° to the chelate ring plane.

Crystals of **11** were shown by X-ray crystallography to have a $C_S$-symmetric structure (Figure 4) very similar to that of **7**. The mirror plane includes the metal center, the two imino groups and the central carbon atoms of the two *tert*-butyl substituents, and so the five-membered chelate ring is flat. The bonding within this ring is similar to that seen in other structures. Another consequence of the mirror symmetry is an absence of the axial/equatorial disposition of the two Fe−X bonds seen in **7**.

Complexes **1**−**13** are all paramagnetic and, with the exceptions of **5** and **6**, afford magnetic moments in the range 4.9−5.1 $\mu_B$, consistent with four unpaired electrons and a quintet ground state.[39−41] The binuclear complexes **5** and **6** afford magnetic moments in the region 3.1−3.4 $\mu_B$ indicating two unpaired electrons and a triplet ground state. Cryoscopic solution molecular weight determinations show that **5** and **6** are aggregated in solution while all the other complexes retain their monomeric structures in solution.

**Cyclic Voltammetry.** Cyclic voltammagrams were recorded on **1**−**13** in acetonitrile using a platinum working and auxiliary electrode with an Ag/AgCl reference electrode and $^nBu_4NPF_6$ (0.1 M) as a supporting electrolyte. Under these conditions the redox potential ($E_{1/2}$) for the $[Cp_2Fe]^{0/+}$ couple occurred at 450 mV, with $\Delta E_p$ = 110 mV; results for **1**−**13** are collected in Table 1.

For the dichloride alkylimine derivatives **1**−**4**, $E_{1/2}$ values lie in the range −60 to −140 mV indicating that the Fe(II) centers are readily oxidized and potentially suited to facile ATRP. Their peak-to-peak separations ($\Delta E_p$) are comparable to the ferrocene-ferrocenium couple, indicating that these $Fe^{II}/Fe^{III}$ couples are facile and reversible. The reversibility of the $Fe^{II}/Fe^{III}$ couple was confirmed by changing the scan rate, upon which a change in the intensities of the anodic and cathodic peaks was observed but no change in their positions. The peak-to-peak separation, $\Delta E_p$, is somewhat larger than the canonical value for ideal Nernstian behavior (59 mV) indicating some reorganization of the coordination sphere of the iron center. This may reflect preferred coordination geometries for each redox state, $Fe^{II}$, $d^6$ and $Fe^{III}$, $d^5$. For the binuclear alkylimine derivatives, **5** and **6**, the $E_{1/2}$ values occur at ca. 800 mV, indicating that these metal centers are much less readily oxidized than those in their mononuclear relatives.

**Table 1. Cyclic Voltammetry Results for Complexes 1−13 (Scheme 1)[a]**

| | $E_{1/2}$/mV | $\Delta E_p$/mV | | $E_{1/2}$/mV | $\Delta E_p$/mV |
|---|---|---|---|---|---|
| **1** | −60 | 120 | **7** | −50 | 220 |
| **2** | −120 | 130 | **8** | −20 | 270 |
| **3** | −140 | 130 | **9** | −40 | 280 |
| **4** | −70 | 120 | **10** | −10 | 290 |
| **5** | 800 | 180 | **11** | 80 | 150 |
| **6** | 820 | 170 | **12** | 70 | 110 |
| | | | **13** | 0 | 260 |

[a] Conditions: acetonitrile, $^nBu_4NPF_6$ (supporting electrolyte, 0.1 M), platinum disk and wire (working and auxiliary electrode), Ag/AgCl (reference electrode) and complex (0.001 M), scan rate 100 mV/s. $E_{1/2}$ is the half-potential for the complex; $\Delta E_p$ is the cathodic−anodic peak separation.

The redox potentials for the arylimine derivatives, **7**−**10**, occurring in the range −10 to −50 mV indicate that these complexes are less reducing than their alkylimine counterparts, consistent with the lower electron donor capacity of the arylimine vs alkylimine donor groups. The large peak-to-peak separations for **7**−**10**, of 200−300 mV, also indicate that the arylimine complexes undergo a more sluggish electron transfer, possibly as a result of a more substantial reorganization of the iron center during the electron-transfer process.

The bromo complexes **11**−**13** possess higher redox potentials than their chloride analogues, e.g., **1**, $E_{1/2}$ = −60 mV and **11**, $E_{1/2}$ = 80 mV. For the alkylimine complexes **11** and **12** the redox couple is reversible ($\Delta E_p$ < 150 mV), but in the case of the aryl derivative **13**, $\Delta E_p$ is again large ($\Delta E_p$ 260 mV), indicating an irreversible or quasi-reversible couple. Thus, the electrochemistry of the alkylimine bromide complexes indicate that they should be well-suited to ATRP catalysis, while their arylimine analogues should facilitate the chain transfer process seen for their chloro relatives.

**Polymerization Studies.** *Styrene Polymerization.* Complexes **1**−**13** were tested for the homogeneous polymerization of styrene (200 equiv) in bulk at 120 °C, under typical ATRP conditions, employing 1-phenylethyl chloride (1-PECl) as an initiator; the results are collected in Table 2.

Polymerizations using **1**−**6** all proceeded via an ATRP mechanism: semilogarithmic plots of $\ln([M]_0/[M]_t)$ vs time (Figure 5a) were linear, indicating that the radical concentration is constant throughout the polymerization.[27,30] Molecular weights increased linearly with conversion (see Figure 5b for **3**/1-PECl) and are in accord with calculated molecular weights. Polydispersities are typically ca. 1.3 and decrease with increasing monomer conversion. Polymerizations catalyzed by **5** and **6** proceeded at significantly slower rates than for **1**−**4** and afforded products with broader molecular weight distributions. A broadened distribution was also observed in the polystyrene samples generated using **1**, a result of tailing to low molecular weight.

**Table 2. Styrene Polymerization Results Using 1-Phenylethyl Chloride (1-PECl) for Complexes 1−13**[a]

| catalyst | % convn | $k_{obs}/h^{-1}$ | $M_{n,th}$ | $M_n$ | $M_w/M_n$ |
|---|---|---|---|---|---|
| **1** | 97 | 0.25 | 20 400 | 18 900 | 1.63[b] |
| **2** | 96 | 0.26 | 20 200 | 20 600 | 1.27 |
| **3** | 99 | 0.31 | 20 900 | 21 600 | 1.21 |
| **4** | 91 | 0.17 | 19 200 | 19 400 | 1.32 |
| **5** | 62 | 0.06 | 13 000 | 14 600 | 1.52 |
| **6** | 39 | 0.02 | 8300 | 8600 | 1.49 |
| **7** | 95 | - | 19 900 | 4700 | 2.08 |
| **8** | 60 | - | 12 500 | 3800 | 1.90 |
| **9** | 60 | - | 12 500 | 3300 | 1.53 |
| **10** | 73 | - | 15 300 | 3400 | 1.60 |
| **11** | 71 | 0.06 | 15 000 | 16 500 | 2.49[b] |
| **12** | 62 | 0.05 | 13 000 | 13 900 | 3.13[b] |
| **13** | 49 | - | 10 300 | 3100 | 1.52 |

[a] Polymerization conditions: 24 h, 120 °C, bulk, [1-PECl]$_0$:[catalyst]$_0$:[styrene]$_0$ = 1:1:200. [b] Low molecular weight tailing. $M_{n,th}$ is the theoretical number-average molecular weight based on the ratio of monomer to initiator, $M_n$ is the observed number-average molecular weight; $M_w/M_n$ is the molecular weight distribution or polydispersity index (PDI).

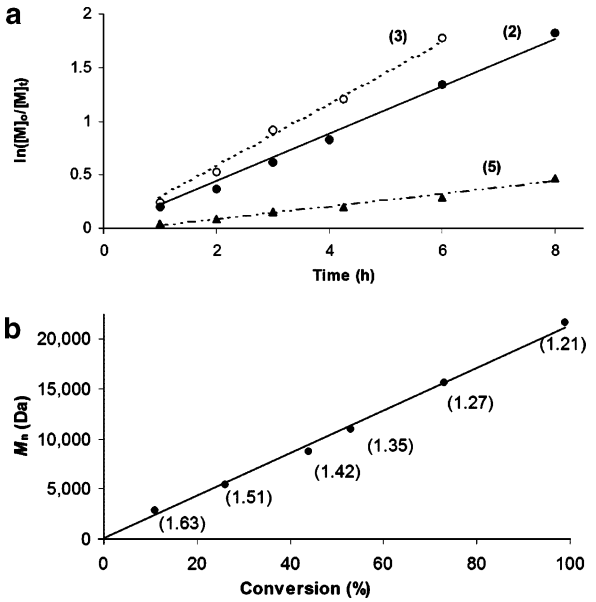


**Figure 5.** (a) Plots of $\ln([M]_0/[M]_t)$ vs time for **2** (○) ($k_{obs}$ = 0.26 $h^{-1}$), **3** (●) ($k_{obs}$ = 0.31 $h^{-1}$), and **5** (▲) ($k_{obs}$ = 0.06 $h^{-1}$) under ATRP conditions (120 °C, bulk, [1-PECl]$_0$:[catalyst]$_0$:[styrene]$_0$ = 1:1:200). (b) Plot of $M_n$ vs conversion ($M_w/M_n$ in parentheses) for complex **3** under ATRP conditions (120 °C, bulk, [1-PECl]$_0$:[**3**]$_0$:[styrene]$_0$ = 1:1:200). $M_n$ is the observed number-average molecular weight; $M_w/M_n$ is the molecular weight distribution or polydispersity index (PDI).

$^1$H NMR analyses of the polystyrene samples generated using **2**−**6** showed the presence of halide end groups (ClC*H*(Ph)$CH_2$ $\delta$ 4.5); this was also supported by halide microanalyses (e.g., for **3**, $M_n$ = 2200; % Cl, found (calcd): 1.48 (1.61)) and MALDI−TOF mass spectrometry on the polymers. For the latter, three families of chains are observed: Cl-terminated/$Ag^+$ vinylene-terminated and vinylene-terminated/$Na^+$. Sodium contamination is a common phenomenon for MALDI−TOF analyses of polymers[42−44] and the observation of vinylene-terminated chains in MALDI−TOF analysis of PS terminated by a halogen function has been reported;[45] the presence of these unsaturated groups was proposed to be due to facile dechlorination upon contact with silver salts.

Chain regrowth experiments provide an important test of a genuine "living" polymerization. In the case of ATRP at elevated temperatures, the reaction can be stopped by lowering the temperature.[46] Figure 6 shows a regrowth experiment using **3**, where styrene was first polymerized at 120 °C over a period of ca. 3 h, and the reaction then stopped by cooling the reaction flask to 0 °C for 10 h. Reheating the sample to the propagation temperature restarted the polymerization at a similar rate, confirming that the total number of growing chains is preserved. The molecular weight ($M_n$) of the polymer before and after the stop, at 11 000 and 11 100 Da, respectively, are identical within experimental error and close to $M_{n,th}$.

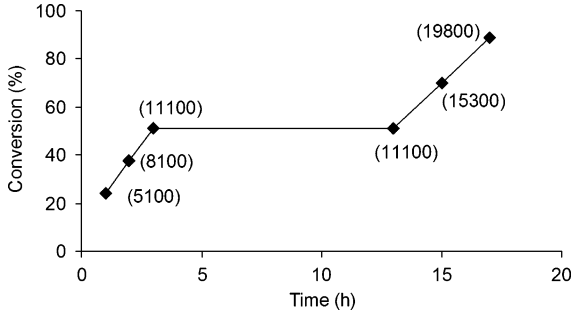


**Figure 6.** Plot of conversion vs time, with $M_n$ in parentheses, for a chain extension experiment using **3**. Conditions: 120 °C, bulk, [1-PECl]$_0$:[**3**]$_0$:[styrene]$_0$ = 1:1:200 with cooling at 3 h to 0 °C for 10 h and then resumption of polymerization at 13 h.

**Table 3. Results for Polymerization of Styrene Catalyzed by 1−3 Utilizing a Variety of Initiators**[a]

| catalyst | initiator | $k_{obs}/h^{-1}$ | $M_{n,th}$ | $M_n$ | $M_w/M_n$ |
|---|---|---|---|---|---|
| **1** | 1−PEBr | 0.05 | 18 300 | 16 700 | 2.23[b] |
| **1** | TosCl | 0.15 | 19 000 | 16 100 | 1.67[b] |
| **1** | PDSC | 0.13 | 19 700 | 16 300 | 2.30[b] |
| **2** | 1−PEBr | 0.11 | 17 100 | 18 200 | 1.29 |
| **2** | TosCl | 0.12 | 19 200 | 19 900 | 1.22 |
| **2** | PDSC | 0.18 | 19 100 | 19 800 | 1.37 |
| **3** | 1−PEBr | 0.09 | 18 700 | 18 500 | 1.39 |
| **3** | TosCl | 0.13 | 19 300 | 19 800 | 1.24 |
| **3** | PDSC | 0.19 | 19 300 | 19 400 | 1.39 |

[a] Polymerization conditions: 120 °C, bulk, [initiator]$_0$:[catalyst]$_0$:[styrene]$_0$ = 1:1:200 (1-PEBr and TosCl) and 0.5:1:200 (PDSC). [b] Indicates a low molecular weight shoulder. $M_{n,th}$ is the theoretical number-average molecular weight based on the ratio of monomer to initiator, $M_n$ is the observed number-average molecular weight; $M_w/M_n$ is the molecular weight distribution or polydispersity index (PDI).

The polymerization of styrene using **1**−**3** was also investigated using other initiators and conditions similar to those described for 1-PECl; results are summarized in Table 3. **1**/1-PEBr resulted in significantly slower polymerizations than for 1-PECl with similar tailing to low molecular weight product. The sulfonyl halide initiators, *p*-toluene sulfonyl chloride (TosCl) and phenoxybenzene disulfonyl chloride (PDSC), gave comparable molecular weight data to samples obtained using 1-PECl, although polymerizations were notably slower. For polymerizations using **2** and **3**, good molecular weight control was achieved ($M_w/M_n$ < 1.4) using all three initiators and molecular weights were close to predicted values. As expected for a radical polymerization, addition of 1.5 mol equivalents of a radical inhibitor, such as galvinoxyl completely retarded the polymerization.

The polymerization of styrene using the aryl-substituted diimine complexes, **7**−**10**, was monitored under similar conditions (120 °C, 200 equiv, bulk, 1-PECl initiator). In these cases the semilogarithmic plots of $\ln([M]_0/[M]_t)$ vs time were nonlinear: $M_n$ did not increase linearly over time and did not agree with theoretical molecular weight values (Figure 7). Monomer conversion, however, did increase in an almost linear manner with time although an induction period of around 30 min was observed. This suggested that a different polymerization mechanism may be operating. Similar polymerization results

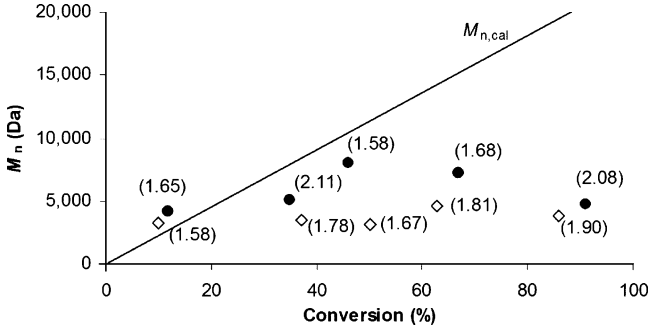


**Figure 7.** Plot of $M_n$ vs conversion for **7** (●) and **8** (◇) with $M_w/M_n$ in parentheses (conditions: 120 °C, bulk, [1-PECl]$_0$:[catalyst]$_0$:[styrene]$_0$ = 1:1:200).

were obtained when a variety of ATRP initiators (e.g., 1-PEBr, TosCl, PDSC) were employed.

Halide microanalyses on the resultant polystyrene polymers showed zero halide content. The absence of a signal ca. $\delta$ 4.5 in their $^1$H NMR spectra attributable to the methine hydrogen of the chlorine containing end group, and the presence of resonances in the olefinic region ca. $\delta$ 6.2−6.4 confirmed that a different polymerization mechanism was occurring. 2D $^1$H COSY NMR spectroscopy showed that the peaks at $\delta$ 6.2−6.4 couple to a resonance at $\delta$ 3.2, attributable to the methine hydrogen adjacent to the double bond. In addition, these signals show correlations to carbon resonances in the region $\delta$ 127−139. This $^{13}$C shift range, together with the $^1$H NMR shifts, is strongly indicative of an olefinic group conjugated to an aromatic ring. When combined with the evidence from MALDI−TOF mass spectrometry, in which olefin-terminated oligomers are clearly resolved, it can be reasonably concluded that these polystyrene samples possess vinylene end groups.

Styrene polymerizations catalyzed by the bromo derivatives **11** and **12** are significantly slower than for their dichloride analogues and are less controlled ($k_{obs}$ = 0.26 h$^{-1}$ and $M_w/M_n$ = 1.27 for **2** vs $k_{obs}$ = 0.05 h$^{-1}$ and $M_w/M_n$ = 2.49 for **12**); they do, however, proceed by an ATRP mechanism, with $M_n$ increasing linearly with conversion and linear first-order kinetics being observed. The polydispersities broaden after ca. 6 h indicating a loss of control. A loss of molecular weight control in copper-based systems when a bromide initiator is used in conjunction with a bromide metal complex has been previously reported;[47] this has been attributed to side-reactions which are more favorable in the bromide initiated and catalyzed systems than those with mixed halides. The aryl dibromide complex, **13**, afforded similar unsaturated product to that obtained using its dichloro analog **8**.

*Methyl Methacrylate Polymerization.* When ethyl-2-bromoisobutyrate (EBrB) is employed as an initiator, MMA polymerizes smoothly in the presence of **1**−**6** in toluene at 80 °C (Table 4).[31] Semilogarithmic plots of ln([M]$_0$/[M]$_t$) vs time were linear in all cases (up to 90% conversion) indicating that the radical concentration is constant throughout the polymerization run. Molecular weights ($M_n$) increase linearly with conversion and with monomer to initiator ratio; a plot of $M_n$ vs monomer to initiator ratio using **3**/EBrB is shown in Figure 8.

Halide analyses indicated the presence of one halogen per polymer chain [e.g., for **4**: $M_n$ = 5400; % Cl, found (calcd): 1.39 (1.48)], while $^1$H NMR spectroscopy confirmed a fully saturated product. However, the methoxy resonance from PMMA dominates the region $\delta$ 3.5−3.9 and obscures the $\omega$-end group resonances. The α-end group is visible as a quartet resonance at $\delta$ 4.1 arising from the methylene protons of the ethyl ester derived from the EBrB initiator. Molecular weights can also be determined by integrating this signal with respect to the PMMA methoxy resonance. Molecular weights close to those determined by GPC analysis are found, e.g., for **3**, $M_{n,NMR}$ = 2100 and $M_{n,GPC}$ = 2300. For the PMMA samples generated by **1**−**6**, the *mm*:*mr*:*rr* ratio (6:34:60) is comparable to that of an AIBN initiated polymerization, indicative of a radical chain growth mechanism.[48−50]

**Table 4. Results of MMA Polymerization for Complexes 1−6**[a]

| catalyst | $k_{obs}$ /h$^{-1}$ | % convn in 24 h | $M_{n,th}$ | $M_n$ | $M_w/M_n$ |
|---|---|---|---|---|---|
| **1** | 0.10 | 79 | 7900 | 9100 | 1.43 |
| **2** | 0.13 | 84 | 8400 | 9000 | 1.21 |
| **3** | 0.16 | 93 | 9300 | 10 100 | 1.19 |
| **4**[b] | 0.06 | 38 | 7600 | 7300 | 1.42 |
| **5**[b] | 0.04 | 33 | 6900 | 9800 | 2.11 |
| **6**[b] | 0.03 | 29 | 6000 | 8100 | 2.20 |

[a] Polymerization conditions: 80 °C, toluene (1:10 toluene/MMA ratio), [EBrB]$_0$:[catalyst]$_0$:[MMA]$_0$ = 1:1:100. [b] [EBrB]$_0$:[catalyst]$_0$:[MMA]$_0$ = 1:1:200. $M_{n,th}$ is the theoretical number-average molecular weight based on the ratio of monomer to initiator, $M_n$ is the observed number-average molecular weight; $M_w/M_n$ is the molecular weight distribution or polydispersity index (PDI).

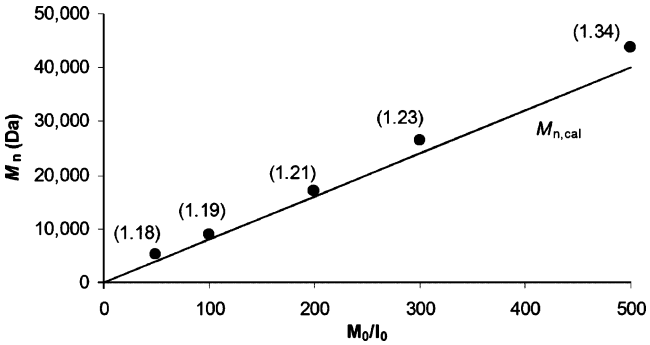


**Figure 8.** Plot of molecular weight vs [M]$_0$/[I]$_0$ for **3** with $M_w/M_n$ in parentheses (conditions: 80 °C, toluene (1:10 w/w ratio), [EBrB]$_0$:[**3**]$_0$:[MMA]$_0$ = 1:1:50, 100, 200, 300, and 500).

**Table 5. MMA Polymerization Results for 2 and 3, Utilizing Various Initiators**[a]

| catalyst | initiator | $k_{obs}$/h$^{-1}$ | $M_{n,th}$ | $M_n$ | $M_w/M_n$ |
|---|---|---|---|---|---|
| **2** | TosCl | 0.15 | 9100 | 11 000 | 1.22 |
| **2** | MBPA | 0.06 | 8300 | 10 500 | 1.16 |
| **2** | DBMM | 0.12 | 8600 | 13 200 | 1.16 |
| **3** | TosCl | 0.14 | 8700 | 10 200 | 1.23 |
| **3** | MBPA | | | | |
| **3** | DBMM | 0.10 | 9100 | 13 700 | 1.15 |

[a] Polymerization conditions: 80 °C, toluene (1:10 w/w ratio), [initiator]$_0$:[catalyst]$_0$:[MMA]$_0$ = 1:1:100. $M_{n,th}$ is the theoretical number-average molecular weight based on the ratio of monomer to initiator, $M_n$ is the observed number-average molecular weight; $M_w/M_n$ is the molecular weight distribution or polydispersity index (PDI).

Complexes **2** and **3** were tested using tosyl chloride (TosCl), methyl-α-bromophenylacetate (MBPA) and diethyl-2-bromo-2-methylmalonate (DBMM) as initiators, respectively, under the same conditions as described using EBrB (Table 5). While MBPA is an unsuitable initiator for the polymerization of MMA in conjunction with **3**, TosCl initiated the ATRP of MMA and gives comparable polymerization results and polymer properties to those obtained using EBrB. The malonate dimer, DBMM, gives similar polymerization kinetics to its monomeric analogue, EBrB. However, the molecular weights are higher than predicted, although there is no accompanying loss in control ($M_w/M_n$ < 1.2). Polymerizations of MMA reported by Sawamoto and co-workers, using this initiator and catalyzed by $FeCl_2$-

**Table 6. Results of MMA Polymerizations Using Catalysts 7−10[a]**

| catalyst | time/h | % convn | $M_{n,th}$ | $M_n$ | $M_w/M_n$ |
|---|---|---|---|---|---|
| **7** | 2 | 8 | 800 | 2700 | 1.56 |
| **7** | 6 | 31 | 3100 | 3800 | 1.59 |
| **7** | 24 | 78 | 7800 | 3600 | 1.49 |
| **8** | 2 | 11 | 1100 | 2300 | 1.55 |
| **8** | 6 | 27 | 2700 | 2000 | 1.47 |
| **8** | 24 | 67 | 6700 | 2200 | 1.50 |
| **9**[b] | 24 | 44 | 8700 | 1900 | 1.58 |
| **10**[b] | 24 | 38 | 7600 | 2100 | 1.65 |

[a] Polymerization conditions: 80 °C, toluene (1:10 w/w ratio), $[EBrB]_0$:$[catalyst]_0$:$[MMA]_0$ = 1:1:100. [b] $[EBrB]_0$:$[catalyst]_0$:$[MMA]_0$ = 1:1:200. $M_{n,th}$ is the theoretical number-average molecular weight based on the ratio of monomer to initiator, $M_n$ is the observed number-average molecular weight; $M_w/M_n$ is the molecular weight distribution or polydispersity index (PDI).

**Table 7. MA Polymerization Results Using 3 and 7[a]**

| catalyst | initiator | $k_{obs}/h^{-1}$ | % convn in 24 h | $M_{n,th}$ | $M_n$ | $M_w/M_n$ |
|---|---|---|---|---|---|---|
| **3** | MBrP | 0.08 | 84 | 7200 | 8400 | 1.53 |
| **3** | 2−BPN | 0.01 | 7 | 600 | − | − |
| **7** | MBrP | − | 62 | 5300 | 1100 | 1.56 |
| **7** | 2−BPN | − | 28 | 2400 | 1200 | 1.63 |

[a] Polymerization conditions: 90 °C, bulk, $[initiator]_0$:$[catalyst]_0$:$[MA]_0$ = 1:1:100. $M_{n,th}$ is the theoretical number-average molecular weight based on the ratio of monomer to initiator, $M_n$ is the observed number-average molecular weight; $M_w/M_n$ is the molecular weight distribution or polydispersity index (PDI).

$(PPh_3)_2$, also resulted in increased molecular weights relative to calculated values.[18]

Polymerizations using the aryl derivatives **7**−**10** with EBrB as an initiator showed that the molecular weights of the resultant polymer samples do not increase linearly with conversion and are not in accord with values calculated on the basis of monomer conversion and monomer-to-initiator ratio. However, monomer conversion does increase in a semilinear manner with time suggesting that a catalytic chain transfer process is occurring. Halide microanalyses of PMMA samples generated using **7**−**10** showed no halide content. Moreover, $^1H$ and $^{13}C$ NMR spectra revealed vinylene end groups and MALDI−TOF analyses indicated the presence of vinylene end-capped polymer chains, with both $Na^+$ and $K^+$ counterions.

**Methyl Acrylate Polymerization.** Complexes **3** and **7** were tested for the polymerization of MA (100 equiv) in bulk at 90 °C using methyl bromopropionate (MBrP) and 2-bromopropionitrile (2-BPN) as initiators; the results are presented in Table 7.

Compound **3** appears to be a reasonable ATRP catalyst for MA when initiated with MBrP. The rate constant, $k_{obs}$, of 0.08 $h^{-1}$ is lower than that observed for MMA, reflecting the less reactive carbon-halogen bond in acrylates.[51] However, the kinetics are linear and molecular weights are close to those predicted based on conversion (Figure 9), though the molecular weight distributions are somewhat broadened relative to PMMA samples generated using the same catalyst. By contrast, the arylimine derivative **7** produces low molecular weight unsaturated product (Figure 9) again indicative of the polymerization being accompanied by efficient chain transfer.

***p*-Methoxystyrene Polymerization.** Polymerizations of styrenes containing strongly electron donating groups, such as methoxy, often proceed by an outer sphere electron transfer (OSET) mechanism which gives rise to heterolysis of the dormant C−Br bond and a cationic polymerization process;[52] as such, *p*-methoxystyrene can be used as a test of a radical vs cationic polymerization pathway. The polymerization of

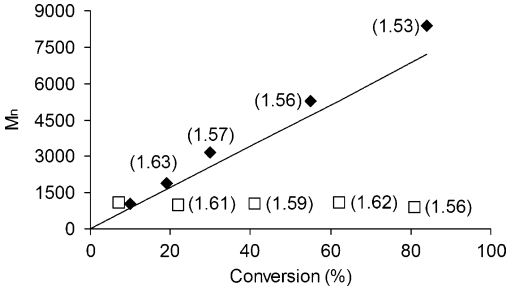


**Figure 9.** Plot of $M_n$ vs conversion with $M_w/M_n$ in parentheses for the polymerization of MA using complexes **3** (◆) and 7 (□) (conditions: 90 °C, bulk, $[MBrP]_0$:$[catalyst]_0$:$[MA]_0$ = 1:1:100).

**Table 8. *p*-OMeSt and Styrene Polymerization Results for 2 and 8 Using 1-PECl as an Initiator[a]**

| catalyst | monomer | $k_{obs}/h^{-1}$ | % conv in 24 h | $M_{n,th}$ | $M_n$ | $M_w/M_n$ |
|---|---|---|---|---|---|---|
| **2** | St | 0.26 | 96 | 20 200 | 20 600 | 1.27 |
| **2** | *p*-OMeSt | 0.20 | 57 | 15 000 | 14 200 | 1.44 |
| **8** | St | | 60 | 12 600 | 3800 | 1.90 |
| **8** | *p*-OMeSt | | 72 | 18 800 | 5200 | 1.96 |

[a] Polymerization conditions: 120 °C, bulk, $[1\text{-PECl}]_0$:$[catalyst]_0$:$[monomer]_0$ = 1:1:200. $M_{n,th}$ is the theoretical number-average molecular weight based on the ratio of monomer to initiator, $M_n$ is the observed number-average molecular weight; $M_w/M_n$ is the molecular weight distribution or polydispersity index (PDI).

**Table 9. Polymerization of MMA in Methanolic Solutions Utilizing Complex 2[a]**

| catalyst | % MeOH | $k_{obs}/h^{-1}$ | $M_{n,th}$ | $M_n$ | $M_w/M_n$ |
|---|---|---|---|---|---|
| **2** | 0 | 0.13 | 8400 | 9000 | 1.21 |
| **2** | 1 | 0.14 | 8500 | 9200 | 1.23 |
| **2** | 5 | 0.28 | 9800 | 10 100 | 1.37 |
| **2** | 50 | 0.36 | 8900 | 11 200 | 1.68 |

[a] Polymerization conditions: 80 °C, toluene and varying concentration of MeOH, $[EBrB]_0$:$[\mathbf{2}]_0$:$[MMA]_0$ = 1:1:100. $M_{n,th}$ is the theoretical number-average molecular weight based on the ratio of monomer to initiator, $M_n$ is the observed number-average molecular weight; $M_w/M_n$ is the molecular weight distribution or polydispersity index (PDI).

*p*-OMeSt was performed using **2** and **8** under identical polymerization conditions to those described for styrene (Table 8). Complex **2** showed good control for the ATRP of *p*-OMeSt with a first-order rate constant, $k_{obs}$, of 0.20 $h^{-1}$. The polymerization rate is slower than that observed for unsubstituted styrene and broader polydispersities were obtained. This is unsurprising due to the electron donating nature of the methoxy substituent which decreases the monomer reactivity and increases the stability of the dormant polymer chain. End group analysis by $^1H$ NMR spectroscopy showed evidence for a halide end group and this was confirmed by chloride microanalysis (e.g., for **2**, $M_n$ = 2100; % Cl, found (calcd): 1.49 (1.68)). Complex **8** gave similar polymerization results for the polymerization of *p*-OMeSt as found for styrene, and molecular weight and polydispersities of the polymers produced were similar in both cases (Table 8). Olefinic end groups were identified in the $^1H$ NMR analysis, suggesting a similar chain transfer mechanism to that observed for styrene.

**Polymerizations in Protic Media.** To establish the viability of polymerizations in methanolic solutions and the effect of the protic solvent on polymerization rate and control, a series of polymerizations were carried out using **2** and methyl methacrylate (MMA) in mixed toluene/methanol solutions (1, 5 and 50% MeOH in toluene). The results are collected in Table 9. **2** is stable in low concentration methanolic solution for prolonged periods at elevated temperatures and gave good polymerization results for MMA in this solvent mix. At a concentration of ca.

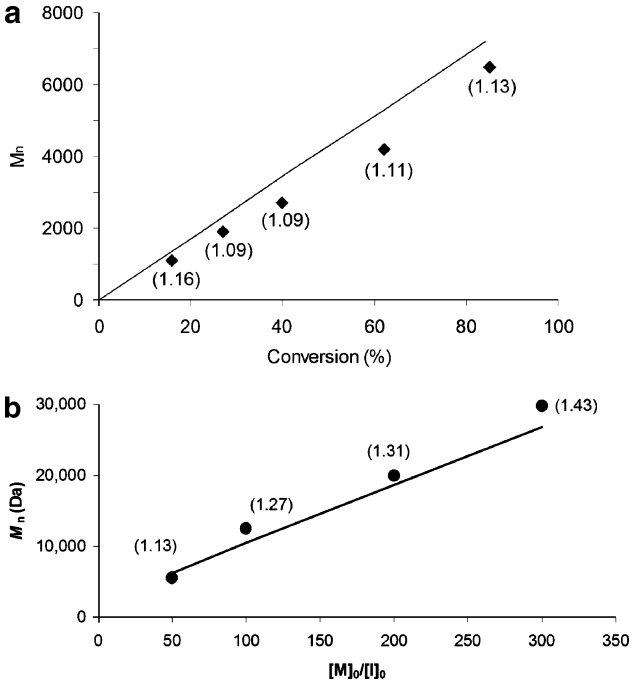


**Figure 10.** (a) HPMA polymerization at 25 °C, plot of $M_n$ vs conversion with $M_w/M_n$ in parentheses (conditions: methanol 50% v/v monomer, $[MBPA]_0$:$[\mathbf{2}]_0$:$[HPMA]_0$ = 1:1:50). (b) Plot of $M_n$ vs $[M]_0/[I]_0$ with $M_w/M_n$ in parentheses for complex **2** (conditions: 25 °C, methanol 50% v/v monomer, $[MBPA]_0$:$[\mathbf{2}]_0$:$[HPMA]_0$ = 1:1:50, 100, 200, 300).

1% relative to toluene, the polymerization behavior is similar to that in toluene but, as the concentration of MeOH is raised, the rate of polymerization increases, though at the expense of molecular weight control.

These promising results encouraged us to investigate the use of **2** for the polymerization of the hydrophilic monomer, HPMA (2-hydroxypropyl methacrylate), in bulk methanol (50 v/v monomer) at 60 and at 25 °C using EBrB as an initiator. Linear kinetics were obtained for both room-temperature polymerizations and also at elevated temperature (60 °C, $k_{obs}$ = 0.13 $h^{-1}$; 25 °C, $k_{obs}$ = 0.03 $h^{-1}$). However, molecular weights deviated significantly from those predicted on the basis of conversion and, since this may be attributable to poor initiator efficiency, methyl-α-bromophenylacetate (MBPA)[53] was employed for further studies. The polymerization of HPMA at 25 °C using **2**/MBPA gave first-order kinetics, with a $k_{obs}$ of 0.08 $h^{-1}$, and a linear increase in $M_n$ with conversion (Figure 10a). A plot of $M_n$ vs $[M]_0/[I]_0$ for differing monomer to initiator ratios revealed a linear relationship indicative of a pseudo-living polymerization (Figure 10b). Raising the polymerization temperature to 60 °C gave a faster rate of polymerization ($k_{obs}$ = 0.46 $h^{-1}$) but the polymerization became less well-controlled ($M_w/M_n$ = 1.36 vs 1.13). At both temperatures, discoloration of the polymerization solution after ca. 6 h is suggestive of catalyst instability upon prolonged exposure to the protic medium.

**Ketimine α-Diimine Iron(II) Complexes: Assessment of Steric vs Electronic Influences.** To confirm whether the observed mechanism switch is due to steric or electronic factors a series of ketimine iron(II) complexes was synthesized and evaluated for styrene polymerization. The ketimine ligands $^{R,Me}[N,N]$ ($^{R,Me}[N,N]$ = RN═C(Me)−C(Me)═NR, R = Cy, Ph, 2,6−$Pr^i_2C_6H_3$ (DiPP)) were complexed to $FeCl_2$ by reaction in $Et_2O$ or benzene for 24 h (NB. a phenylimine derivative did not prove accessible in the aldimine series). $^{Cy,Me}[N,N]FeCl_2$, **14**, $^{Ph,Me}[N,N]FeCl_2$, **15**, and $^{DiPP,Me}[N,N]FeCl_2$, **16**, were isolated as microcrystalline solids in good yields and characterized by elemental analysis, mass spectrometry, IR ($\upsilon$(C═N) = 1590 to 1640 $cm^{-1}$) and magnetic moment measurements (5.0−5.1 $\mu_B$).

**Table 10. Styrene Polymerization Results for 14−16[a]**

| catalyst | $k_{obs}/h^{-1}$ | % convn in 24 h | $M_{n,th}$ | $M_n$ | $M_w/M_n$ |
|---|---|---|---|---|---|
| **14** | 0.17 | 93 | 19 500 | 18 600 | 1.48 |
| **15** | | 86 | 18 100 | 4000 | 1.53 |
| **16** | | 72 | 15 100 | 3800 | 1.71 |

[a] Polymerization conditions: 120 °C, bulk, $[1\text{-PECl}]_0$:$[catalyst]_0$:$[styrene]_0$ = 1:1:200. $M_{n,th}$ is the theoretical number-average molecular weight based on the ratio of monomer to initiator, $M_n$ is the observed number-average molecular weight; $M_w/M_n$ is the molecular weight distribution or polydispersity index (PDI).

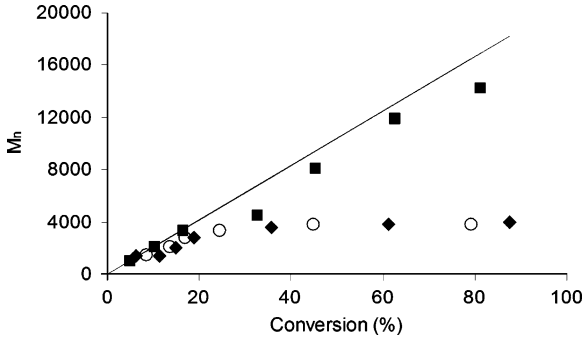


**Figure 11.** Plot of $M_n$ vs conversion for styrene polymerizations using complexes **14** (■), **15** (◆), and **16** (○). Conditions: 120 °C, bulk, $[1\text{-PECl}]_0$:$[catalyst]_0$:$[styrene]_0$ = 1:1:200).

Complex **15** lacks the *ortho* substituents on the phenyl ring present in DiPP and mesityl catalyst derivatives. The steric environment in this catalyst precursor should be reasonably similar to the cyclohexylimine catalyst **14**, and, if anything slightly less crowded due to the $sp^2$-hybridized character of the *ipso* carbon of the phenyl substituent. If an electronic effect drives the switch in polymerization mechanism from ATRP to CCT, the electron-withdrawing ligand of **15** should match the observed polymerization mechanism of the DiPP-substituted catalyst **16**. To investigate this trend, complexes **14**−**16** were tested for the ATRP of styrene (Table 10).

Complex **14** afforded reasonable ATRP behavior (linear polymerization kinetics and predominantly halogen-terminated polymer chains), although at a slightly slower rate than for its aldimine relatives. Contrastingly, **15** and **16** gave similar results to those reported for the aryl-substituted aldimine complexes, with low molecular weight polymers produced independent of the degree of conversion (Figure 11).

**Related Four-Coordinate Iron(II) Complexes: Diamine and Diphosphine Derivatives.** With a view to optimizing catalyst performance and obtaining a better understanding of the factors influencing the performance of four-coordinate iron catalysts, the study was extended to tertiary diamine and diphosphine derivatives. The diamine adduct **17** was prepared by a modification of reported procedures,[54,55] involving treatment of *N*,*N*,*N*′,*N*′-tetraethylethylenediamine (TEEDA) with $FeCl_2$. Pale green **17** is a highly oxygen and moisture sensitive, paramagnetic ($\mu_{eff}$ = 5.12 $\mu_B$) crystalline solid, but is monomeric, in contrast to its less hindered TMEDA relative, $[\{FeCl(TMEDA)\}_2(\mu\text{-}Cl)_2]$.[54] The X-ray structure of **17** is shown in Figure 12, and reveals a distorted tetrahedral geometry with inter-bond angles in the range 83.71(10)−120.09(5)°, the acute angle being associated with the bite of the *N*,*N*′-chelate ligand. The bond lengths and angles are unexceptional, save for an enlargement of the Cl(1)−Fe−Cl(2) angle [120.09(5) Å] and a

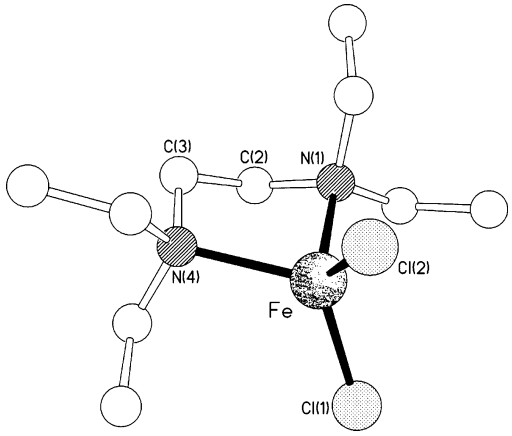


**Figure 12.** Molecular structure of **17**. Selected bond lengths (Å) and angles (deg); Fe−N(1) 2.151(3), Fe−N(4) 2.192(3), Fe−Cl(2) 2.2296(11), Fe−Cl(1) 2.2399(11), N(1)−C(2) 1.485(4), C(2)−C(3) 1.514(5), C(3)−C(4) 1.499(4), N(1)−Fe−N(4) 83.71(10), N(1)−Fe−Cl(2) 116.78(8), N(4)−Fe−Cl(2) 110.05(8), N(1)−Fe−Cl(1) 106.46(8), N(4)−Fe−Cl-(1) 114.19(8), Cl(2)−Fe−Cl(1) 120.09(5).

narrowing of the N(1)−Fe−N(4) angle [83.71(10) Å] from an ideal tetrahedral geometry due to the strain imposed by the five-membered chelate ring.

The bidentate phosphine complexes **18**−**22** (**18**, R = $^{i}$Pr; **19**, R = $C_6H_5$; **20**, R = $C_6F_5$; **21**, R = Cy; **22**, R = Et) were isolated in good yields upon treatment of the diphosphine with $FeCl_2$ or $FeCl_2(THF)_{1.5}$ in THF or toluene. **18** and **19** have been reported previously,[56−58] while **22** was previously reported to be a bis-chelate complex.[59] Complexes **18**−**21** were isolated as off-white paramagnetic solids, with magnetic moments in the range 5.0−5.5 $\mu_B$, and elemental analyses and mass spectra consistent with the formation of mono-chelate high spin Fe(II) complexes. In contrast to the bis(chelate) structure favored for the complex containing the bis-diethylphosphinoethane ligand, the secondary alkyl phosphorus substituents in **18** and **21** appear to afford sufficient steric hindrance to stabilize a mononuclear four-coordinate complex, confirmed by a single-crystal structure determination on **21** (Figure 13). Complex **21** crystallizes with two independent molecules in the unit cell, each having essentially identical conformations. The geometry at the iron center is in both cases distorted tetrahedral with bond angles in the range 83.91(5)−115.99(6)° and 83.85(5)−116.11(6)°, in molecules **A** and **B** respectively, the acute angle in each case being associated with the chelate bite. The chelate ring has an asymmetric folded geometry approaching an envelope conformation with the methylene carbon atoms C(1) and C(2) lying respectively 0.39 and 0.15 Å, [0.43 and 0.13 Å, molecule **B**] "above" and "below" the $FeP_2$ plane.

Complexes **17**−**20** and **22** were analyzed by cyclic voltammetry under identical experimental conditions to those described for their diimine relatives and the results are presented in Table 11. Meaningful measurements could not be obtained on **21** due to its insolubility in acetonitrile. The mononuclear diamine complex **17** shows favorable electrochemistry compared to its unsaturated diimine counterparts (cf. **2** $E_{1/2}$ = −120 mV) and the redox couple is accessible and reversible. While the iron(II) phosphine complexes **18**−**20** and **22** exhibit low redox potentials, a consequence of their highly electron-donating phosphine ligands, they all show large peak-to-peak separations, $\Delta E_p$, in the range 270−380 mV. In addition, on changing the scan rate, both the position and intensity of the cathodic and anionic peaks, $E_{pc}$ and $E_{pa}$, changed indicating that the redox couples in **18**−**20** and **22** are not reversible.

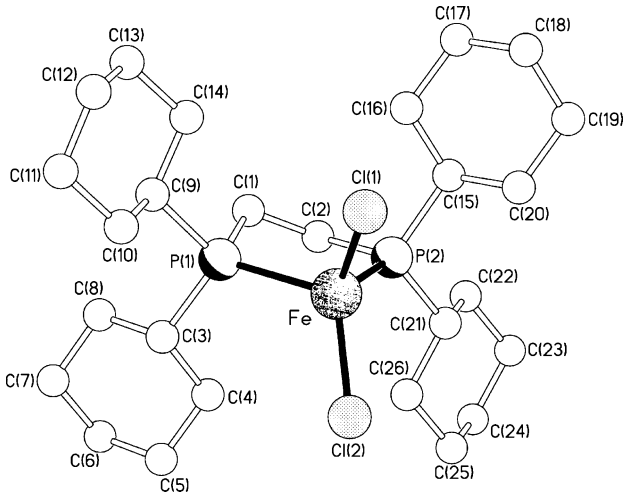


**Figure 13.** Structure of one (**A**) of the two independent molecules present in the crystals of **21**. Selected bond lengths (Å) and angles (deg) for independent molecules **A** and **B**; **A**: Fe−Cl(1) 2.2345(14), Fe−Cl(2) 2.2277(14), Fe−P(1) 2.4614(14), Fe−P(2) 2.4660(14), Cl(1)−Fe−Cl(2) 114.76(6), Cl(1)−Fe−P(2) 112.37(5), Cl(2)−Fe−P(2) 114.82(6), Cl(1)−Fe−P(1) 111.31(5), Cl(2)−Fe−P(1) 115.99(6), P(1)−Fe−P(2) 83.91(5). **B**: Fe−Cl(1) 2.239(2), Fe−Cl(2) 2.220(2), Fe−P(1) 2.456(2), Fe−P(2) 2.4656(14), Cl(1)−Fe−Cl(2) 115.62(7), Cl(1)−Fe−P(2) 112.08(6), Cl(2)−Fe−P(2) 114.71(6), Cl(1)−Fe−P(1) 110.44(6), Cl(2)−Fe−P(1) 116.11(6), P(1)−Fe−P(2) 83.85(5).

**Table 11. Cyclic Voltammetry Data for Complexes 17−20 and 22[a]**

| complex | $E_{1/2}$/mV | $\Delta E_p$/mV |
|---|---|---|
| **17** | −160 | 120 |
| **18** | −210 | 280 |
| **19** | −200 | 350 |
| **20** | −200 | 270 |
| **22** | −290 | 380 |

[a] Conditions: acetonitrile, $^{n}Bu_4NPF_6$ (supporting electrolyte, 0.1 M), platinum disk and wire (working and auxiliary electrode), Ag/AgCl (reference electrode) and complex (0.001 M), scan rate 100 mV/s. $E_{1/2}$ is the half-potential for the complex; $\Delta E_p$ is the cathodic−anodic peak separation.

**Table 12. Styrene Polymerization Results for 17−22[a]**

| catalyst | $k_{obs}/h^{-1}$ | % convn in 24 h | $M_{n,th}$ | $M_n$ | $M_w/M_n$ |
|---|---|---|---|---|---|
| **17** | 0.19 | 99 | 20 900 | 18 700 | 1.40 |
| **18** | | 26 | 10 100 | 900 | 2.63 |
| **19** | | 23 | 9000 | 990 | 3.75 |
| **20** | | 25 | 9500 | 1000 | 2.58 |
| **21** | | 28 | 10 100 | 800 | 2.96 |
| **22** | | 26 | 10 000 | 800 | 2.74 |

[a] Polymerization conditions: 120 °C, bulk, [1-PECl]$_0$:[catalyst]$_0$:[styrene]$_0$ = 1:1:200. $M_{n,th}$ is the theoretical number-average molecular weight based on the ratio of monomer to initiator, $M_n$ is the observed number-average molecular weight; $M_w/M_n$ is the molecular weight distribution or polydispersity index (PDI).

**Polymerization Studies.** Complexes **17**−**22** were tested for the ATRP of styrene (200 equiv) at 120 °C using 1-PECl as an initiator (Table 12). Polymerizations using the saturated diamine complex, **17**, were found to proceed in a *pseudo*-living manner, affording first-order kinetics with respect to monomer concentration and a linear increase in molecular weight with conversion. The isolated polystyrene samples were found to be halide-terminated (by $^1$H NMR). By contrast, styrene polymerizations using **18**−**22** were uncontrolled with low molecular weight polymers being obtained independent of the degree of conversion. The kinetics did not increase in a linear manner with time and low conversions (ca. 25%) resulted after 24 h.

Polymerizations under similar conditions, but using 1-PEBr as the initiator, gave similar results. For **17**, $k_{obs} = 0.17\ h^{-1}$, with similar molecular weight control ($M_n = 18{,}400$, $M_{n,th} = 20\ 100$) and polydispersity ($M_w/M_n = 1.35$) to those found using 1-PECl.

MMA polymerizations (100 equiv) at 80 °C, using EBrB as an initiator in toluene (1:10 w/w ratio) were unsuccessful using **18**−**22**; the polymerization results were similar to those reported for styrene, with nonlinear kinetics and low molecular weight products produced throughout the polymerizations. Complex **17** gave good polymerization results, with $k_{obs} = 0.11\ h^{-1}$ and $M_n = 11\ 800$, $M_{n,th} = 9800$; $M_w/M_n = 1.25$.

## Discussion

Since the discovery of transition metal complexes capable of mediating atom transfer radical polymerization, and the demonstration of the plethora of materials accessible using this methodology,[1,2] there has been much interest in developing catalyst systems suitable for industrial application. A commercially exploitable ATRP catalyst needs to address a number of important aspects, including the toxicity of the metal and its attendant ligand(s), the color of the metal complex, catalyst robustness and efficiency. For robust and efficient catalysts, a balance between several different parameters must be achieved: ideally the ground state of the reduced species should be stable to air and moisture; it should be sufficiently halogenophilic to provide a thermodynamic driving force to "capture" the halogen end group attached to the initiator and the growing polymer chain; the oxidized species should also ideally be stable to air and moisture, but be sufficiently high in energy relative to the reduced species to maintain a low equilibrium concentration of polymer radicals.

Catalyst color can be a demanding criterion since many late transition metal catalysts bearing unsaturated nitrogen ligands engage in extensive metal-to-ligand charge transfer and are consequently highly colored. Lightly colored catalysts are desirable or, alternatively, efficient procedures for the separation of colored catalyst residues need to be employed. In situ oxidation of the catalyst post-polymerization provides an alternative strategy to eliminate colored impurities from the isolated polymers. The biological toxicity of the metal is also important, especially so for materials designed for in vivo applications. Copper is less attractive in this regard, while iron holds a special appeal due to the body's natural iron storage and transport capacities. This study has focused primarily on four-coordinate iron(II) dichloride complexes bearing a bidentate neutral α-diimine donor ligand. Oxidation of these species in air or by precipitation of the polymer into acidified methanol leads to rapid decoloration, releasing biocompatible iron and relatively benign amines and aldehydes via ligand hydrolysis.

Four-coordinate complexes were reasoned to be more readily able to accommodate a halogen atom than five-coordinate species and also to have greater geometrical flexibility in the oxidized species, thus allowing the oxidized form of the catalyst to access a coordination geometry possibly more suited to dissociative loss of halogen.[28] In most cases, α-diimines were found to react with $FeX_2$ to give $C_2$-symmetric four-coordinate complexes (**1**−**4**). They are air and moisture stable and thermally robust. However, if a less bulky alkyl substituent within the α-diimine ligand is used, this leads to dimeric complexes with five-coordinate geometries, in both the solid and solution state (**5** and **6**).

Redox potentials have been correlated to the effectiveness of ATRP catalysts, with the most reducing complex being the most active catalyst. This is also seen for the diimine iron(II) complexes; for **1**−**4** their redox potentials correlate with the rate of ATRP activity, with the most strongly reducing catalyst being the most active for ATRP while the arylimine complexes were found to have high redox potentials but larger peak-to-peak ($\Delta E_p$) separations indicative of more substantial rearrangements of the metal coordination sphere during the redox cycle.

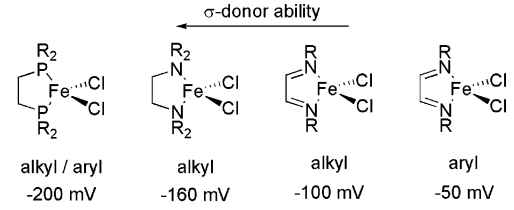


**Figure 14.** Correlation of ligand σ-donating capacity with redox potential, $E_{1/2}$ (mV).

To aid in the understanding of the requirements for the ligand, other bidentate nitrogen and phosphorus ligands attached to iron(II) were investigated. The primary advantages of utilizing these ligands is their commercial availability as well as the pale color of the resultant iron(II) complexes. As was the case for the diimines, a bulky ligand is required to prevent bis-chelation or binucleation.

The CV data confirm the greater reducing power of derivatives containing more electron-donating ligands (Figure 14). However, the correlation does not directly extend to the quality of an ATRP catalyst. The reversibility of the redox couple is also important. For example in the case of the iron(II) phosphine complexes the redox potential is very low ($E_{1/2}$ ca. −200 mV) but the peak-to-peak separation is large ($\Delta E_p$ ca. 300 mV) and as a result the redox couple is not reversible. Other factors must also be considered such as the temperature of operation, and the air and moisture sensitivity of these complexes, (*cf.* diamines vs diimines) which may have a bearing on the activity in ATRP.

**Polymerizations.** Iron(II) diimine complexes bearing alkylimine substituents have proved to be highly effective ATRP catalysts for styrene polymerization, affording polymers with low polydispersities and molecular weights close to calculated values. These polymerizations can be reactivated in a "stop-go" manner indicating that the polymerization has living characteristics. However, ligands bearing less bulky alkyl substituents lead to binuclear complexes with five-coordinate iron centers, and these are less effective ATRP catalysts. By contrast, catalysts containing arylimine substituents do not behave as ATRP catalysts for the polymerization of styrene. Regardless of the size of the aryl substituent on the diimine, low molecular weight polymers are produced. End group analyses and polymerization results are consistent with a β-hydrogen elimination process, such as catalytic chain transfer (CCT). Since CCT processes are traditionally challenging for monosubstituted alkenes such as styrene, an outer sphere electron transfer (OSET) mechanism was also considered.[60−62] Oxidation of the polystyryl radicals to the corresponding cations followed by $\beta$-$H^+$ loss could generate the observed olefin-terminated polymer chains. CuBr/bipy catalyst systems have been shown to operate via OSET mechanisms[52] in the polymerization of the more-readily oxidized *p*-methoxystyrene (*p*-OMeSt). Since *p*-OMeSt is more easily oxidized than styrene, an OSET process should generate poly(*p*-OMeSt) with molecular weights much lower than those of PS formed using catalysts **7**−**10**. However, similar molecular weights were observed for PS and poly(*p*-OMeSt) in all cases suggesting that CCT is the predominant mechanistic pathway.

Polymerizations of styrene by the ketimine derivatives **14**−**16** allowed delineation of the steric and electronic effects in ATRP vs CCT polymerization. The phenyl derivative $^{Ph,Me}$[*N*,*N*]$FeCl_2$, **15**, is sterically quite similar to the ATRP catalyst $^{Cy,Me}$[*N*,*N*]$FeCl_2$, **14**, while being electronically similar to the CCT catalyst $^{DiPP,Me}$[*N*,*N*]$FeCl_2$, **16**. Since **15** polymerizes styrene by a CCT mechanism, this provides direct evidence for electronic, not steric, factors dictating the polymerization pathway in these catalyst systems. Subsequent work has shown that the metal spin-state plays a key role in determining the mechanistic pathway.[32,33]

The iron(II) diamine complex, **17,** is also an effective ATRP catalyst for styrene. The polymerization rate is slower than for iron(II) diimine systems, despite the more accessible redox couple, possibly due to the lower stability of the diamine derivative relative to the diimines in solution and at elevated temperatures. The phosphine complexes, **18**−**22**, are poor ATRP catalysts, despite their very favorable redox potentials, due to the irreversible nature of the $Fe^{II}/Fe^{III}$ couple as evidenced by the large peak to peak separations.

The methacrylate and acrylate polymerizations for the alkylimines and arylimines were similar to those obtained for styrene. Closely related polymerization effects and vinylene end groups were observed in MMA polymerizations using **7**−**10**, indicative of a CCT mechanism. The catalyst concentration of **7** was increased 4-fold under otherwise standard polymerization conditions, whereupon the molecular weight decreased from $M_n$ = 3600 (catalyst concentration 0.1 mM) to $M_n$ = 1100 (catalyst concentration 0.4 mM).[31] This trend, where a decrease in $M_n$ is observed with increasing [Fe] is not observed in MMA polymerizations using **1**−**6**. Further studies show that if an AIBN-initiated polymerization is carried out in the presence of **7**−**10**, greatly reduced molecular weights are obtained. While an AIBN initiated polymerization of 100 equiv of MMA in the absence of catalyst afforded a molecular weight of ca. 35 000 ($M_w/M_n$ = 2.91), the same polymerization in the presence of **7** gave a molecular weight of ca. 6000 ($M_w/M_n$ = 1.70). This experiment clearly differentiates between a CCT and an OSET mechanism, since only $Fe^{II}$ is added to the polymerization mixture and OSET requires electron transfer to $Fe^{III}$ species. These observations are consistent with the iron(II) α-diimine complexes bearing aryl substituents acting as CCT reagents in the polymerization of MMA.

## Conclusions

A family of iron-based ATRP catalysts bearing α-diimine, diamine and diphosphine ligands has been described and characterized. Cyclic voltammetric studies on derivatives containing diimine ligands bearing alkyl substituents reveal reversible one-electron redox couples with $E_{1/2}$ values suitable for their use as ATRP catalysts. Styrene, methyl methacrylate, and methyl acrylate are polymerized in a controlled manner by these alkylimine-based catalysts. Catalysts bearing arylimine substituents afford one-electron redox couples with larger peak to peak separations and resulted, somewhat unexpectedly, in efficient chain transfer processes during the polymerization of styrene and methyl methacrylate. Mechanistic studies strongly indicate that catalytic chain transfer occurs in the case of methyl methacrylate and styrene, rather than an outer sphere electron-transfer mechanism. Related four-coordinate iron(II) complexes, bearing diamine and diphosphine ligands, while affording metal centers of greater reducing power, were less controlled ATRP catalysts, in the case of the diamine derivative possibly due to catalyst instability, while for the diphosphine catalysts due to poor redox reversibility. The iron(II) alkylimine complexes possess reasonable stability in protic media at elevated temperatures allowing polymerizations of HPMA in methanol at 25 and 60 °C, with fast polymerization rates and good molecular weight control.

## Experimental Section

**General Data.** All manipulations were performed by means of standard high vacuum Schlenk and cannula techniques under an atmosphere if nitrogen. Solvents were refluxed over an appropriate drying agent and distilled and degassed prior to use. Crystal data were collected on Siemens P4/PC or P4/RA diffractometers. $^1$H NMR spectra were recorded on a Bruker AC-250 MHz spectrometer at 293 K; chemical shifts are referenced to the residual proton impurity of the deuterated solvent. Infrared spectra were obtained with thin sample films on NaCl plates or as KBr discs on a Perkin-Elmer 1710X FT-IR spectrometer. Mass spectra were recorded on either a VG Autospec, VG Platform II spectrometer or a Bruker Reflex MALDI-tof mass spectrometer. Elemental analyses were performed by the microanalytical services of the Chemistry departments of London Metropolitan University and University College London. $^1$H NMR analyses of polymer end groups were performed at BP Chemicals, Sunbury-on-Thames on a Jeol GSX 270 spectrometer. Magnetic susceptibilities were determined by the Evans NMR method (solvent, $CD_2Cl_2$; reference, cyclohexane). Gel permeation chromatography was performed using Viscotek Trisec software connected to a Knauer differential refractometer. Cyclic voltammetry measurements was obtained using a MacLab potentiostat operated by EChem 1.3.2. software. The working electrode and reference electrode were purchased from Bioanalytical (ref: MF-2013 and RE-5B). Molecular weight determination in solution were determined using melting point depression by means of a TC Ltd platinum resistance thermometer mounted coaxially in a vacuum jacketed cell cooled in an ice bath. The thermometer was connected to an Autotherm II instrument interfaced to a PC-486 running the Mettler Toledo Balance Link software program (Version 3.01).

Styrene and *p*-methoxystyrene were purified by vacuum distillation and then stored under an inert atmosphere over 4 Å molecular sieves at −15 °C. Methyl methacrylate and methyl acrylate were stirred over calcium hydride for 24 h and then vacuum-transferred, degassed and then stored in an inert atmosphere over 4 Å molecular sieves at −15 °C. 2-Hydroxypropyl methacrylate was passed through a basic alumina column and then stirred over $MgSO_4$, transferred to a sealed ampule over 4 Å molecular sieves and degassed by repeated freeze−pump−thaw cycles. Initiators were purified by drying over calcium hydride or molecular sieves and vacuum transferred into sealed Young's tap ampules and degassed thoroughly before use. 2,2′-Azobis(isobutyronitrile) (AIBN) was purified by recrystallization three times from $Et_2O$ and stored at −15 °C. 1-Phenylethyl chloride (1-PECl) and phenyldisulphonyl chloride (PDSC) were synthesized according to literature methods and purified by column chromatography and Soxhlet extraction into toluene respectively.[63,64] The α-diimine ligands were prepared as described in the literature for the alkylimine[30,37,65] and arylimine derivatives.[38,65] The alkyl and aryl ketimine ligand precursors were prepared using modified literature procedures.[66,68] *N*,*N*,*N*′,*N*′-Tetraethylenethanediamine (TEEDA) was dried by refluxing over sodium and then freshly distilled. $(^iPr)_2PCH_2CH_2P(^iPr)_2$ was prepared according to published procedures.[69] All other chemicals were obtained commercially and used as received unless stated otherwise.

**Polymerizations.** All polymerizations were set up and performed under an atmosphere of oxygen-free, dry nitrogen using standard Schlenk-line techniques. In an ampule equipped with a magnetic stirrer bar, the following were placed in order: monomer, initiator and catalyst and solvent in various ratios and then sealed. In all cases the catalyst was soluble in the monomer solution. The ampules were heated in an oil bath, at 120 °C for styrene polymerizations, with magnetic stirring. After stirring for the allotted period of time, an aliquot (0.1 mL) was removed and quenched with THF (1 mL).

Conversion was determined by integration of the monomer vs polymer backbone resonances in the $^1$H NMR spectrum of the crude product in $CDCl_3$. After completion of the reaction, usually 24 h, the contents of the ampules were dissolved in THF. This solution was added dropwise to an approximately 20-fold excess of rapidly stirred acidified methanol (1% HCl v/v). The precipitate that formed was filtered and washed with methanol (3 × 20 mL). The precipitate was dried for 24 h in a vacuum oven at 60 °C. Samples were then analyzed by GPC.

For methyl methacrylate and methyl acrylate, polymerizations were carried out as described for styrene polymerization except the ampules were heated in an oil bath, at 80 °C for MMA in toluene (10% w/w ratio) and 90 °C in bulk for MA polymerizations.

Polymerizations of hydroxypropyl methacrylate were performed under dinitrogen, in a 15 cm$^3$ glass ampule fitted with a Teflon stopcock. The ampule was equipped with a magnetic stir bar and the following were placed in it in the order: monomer, solvent, initiator, and catalyst in a 50:50:1:1 ratio. The ampules were transferred to a preheated oil bath, at 60 °C or 25 °C. After the reactions were stirred for the allotted period of time an aliquot (0.1 mL) was removed and quenched by cooling to −78 °C. Conversion was determined by integration of monomer vs polymer backbone resonances in the $^1$H NMR spectrum of the crude product (in methanol-$d_4$).

**Acknowledgment.** BP Chemicals and NSERC of Canada are thanked for financial support. Dr. Jane Boyle is thanked for NMR measurements. Miss C. Galmes is thanked for assistance with MALDI−TOF mass spectra. Prof. S.P. Armes and Dr. L. Pilon are thanked for advice regarding the hydrophilic monomer polymerizations and for providing samples of HPMA monomer. Prof. F. G. N. Cloke and Dr. G. K. B. Clentsmith are thanked for assistance with cryoscopic molecular weight determinations.

**Supporting Information Available:** Text giving experimental details for the synthesis and characterization of complexes **1**−**22**, figures giving CV trace, $^1$H NMR spectra, plots of $M_n$ vs time, plots of $\ln([M]_0/[M]_t)$ vs time, 2D COSY of PMMA, $^{13}$C NMR spectra, plots of $M_n$ vs conversion, and HPMA polymerization, and tables of polymerization procedures and polymerization data. This material is available free of charge via the Internet at http://pubs.acs.org. CCDC reports 630714−630719, for the X-ray structures of **3**, **5**, **7**, **11**, **17** and **21**, respectively, are available. Contact the author or Cambridge Crystallographic Data Centre for more information.

## References and Notes

(1) Matyjaszewski, K.; Xia, J. *Chem. Rev.* **2001**, *101*, 2921−2990.
(2) Kamigaito, M.; Ando, T.; Sawamoto, M. *Chem. Rev.* **2001**, *101*, 3689−3745.
(3) Wang, J.-S.; Matyjaszewski, K. *J. Am. Chem. Soc.* **1995**, *117*, 5614−5615.
(4) Ando, T.; Kato, M.; Kamigaito, M.; Sawamoto, M. *Macromolecules* **1996**, *29*, 1070−1072.
(5) Haddleton, D. M.; Jasieczek, C. B.; Hannon, M. J.; Shooter, A. J. *Macromolecules* **1997**, *302*, 2190−2193.
(6) Haddleton, D. M.; Clark, A. J.; Duncalf, D. J.; Heming, A. M.; Kukulj, D.; Shooter, A. J. *J. Chem. Soc., Dalton Trans.* **1998**, 381−385.
(7) Haddleton, D. M.; Kukulj, D.; Duncalf, D. J.; Heming, A. M.; Shooter, A. J. *Macromolecules* **1998**, *31*, 5201−5205.
(8) Xia, J. H.; Matyjaszewski, K. *Macromolecules* **1997**, *30*, 7697−7700.
(9) Xia, J.; Gaynor, S. G.; Matyjaszewski, K. *Macromolecules* **1998**, *31*, 5958−5959.
(10) Xia, J.; Matyjaszewski, K. *Macromolecules* **1999**, *32*, 2434−2437.
(11) Wan, X. L.; Ying, S. K. *J. Appl. Polym. Sci.* **2000**, *75*, 802−807.
(12) Göbelt, B.; Matyjaszewski, K. *Macromol. Chem. Phys.* **2000**, *201*, 1619−1624.
(13) Destarac, M.; Bessière, J.-M.; Boutevin, B. *Macromol. Rapid Commun.* **1997**, *18*, 967−974.
(14) Kickelbick, G.; Matyjaszewski, K. *Macromol. Rapid Commun.* **1999**, *20*, 341−346.
(15) Inoue, Y.; Matyjaszewski, K. *Macromolecules* **2004**, *37*, 4014−4021.
(16) Matyjaszewski, K.; Coca, S.; Gaynor, S. G.; Wei, M.; Woodworth, B. E. *Macromolecules* **1997**, *30*, 7348−7350.
(17) Kickelbick, G.; Matyjaszewski, K. *New J. Chem.* **2002**, *26*, 462−468.
(18) Ando, T.; Kamigaito, M.; Sawamoto, M. *Macromolecules* **1997**, *30* 4507−4510.
(19) Takahashi, H.; Ando, T.; Kamigaito, M.; Sawamoto, M. *Macromolecules* **1999**, *32*, 3820−3823.
(20) Ando, T.; Kamigaito, M.; Sawamoto, M. *Macromolecules* **2000**, *33*, 5825−5829.
(21) Kamigaito, M.; Watanabe, Y.; Ando, T.; Sawamoto, M. *J. Am. Chem. Soc.* **2002**, *124*, 9994−9995.
(22) Simal, F.; Demonceau, A.; Noels, A. F. *Angew. Chem., Int. Ed.* **1999**, *38*, 538−540.
(23) Fuji, Y.; Ando, T.; Kamigaito, M.; Sawamoto, M. *Macromolecules* **2002**, *35*, 2949−2954.
(24) Matyjaszewski, K.; Wei, M.; Xia, J.; McDermott, J. E. *Macromolecules* **1997**, *30*, 8161−8164.
(25) Teodorescu, M.; Gaynor, S. G.; Matyjaszewski, K. *Macromolecules* **2000**, *33*, 2335−2339.
(26) Britovsek, G. B. P.; Bruce, M.; Gibson, V. C.; Kimberley, B. S.; Maddox, P. J.; Mastroianni, S.; McTavish, S. J.; Redshaw, C.; Solan, G. S.; Strömberg, S.; White, A. J. P.; Williams, D. J. *J. Am. Chem. Soc.* **1999**, *121*, 8728−8740.
(27) Gibson, V. C.; O'Reilly, R. K.; Wass, D. F.; White, A. J. P.; Williams, D. J. *J. Chem. Soc., Dalton Trans.* **2003**, 2824−2830.
(28) O'Reilly, R. K.; Gibson, V. C.; White, A. J. P.; Williams, D. J. *Polyhedron* **2004**, *23*, 2921−2928.
(29) Zhang, H.; Schubert, U. S. *Chem. Commun.* **2004**, 858−859.
(30) Gibson, V. C.; O'Reilly, R. K.; Reed, W.; Wass, D. F.; White, A. J. P.; Williams, D. J. *Chem. Commun.* **2002**, 1850−1851.
(31) Gibson, V. C.; O'Reilly, R. K.; Wass, D. F.; White, A. J. P.; Williams, D. J. *Macromolecules.* **2003**, *36*, 2591−2593.
(32) Shaver, M. P.; Allan, L. E. N.; Rzepa, H. S.; Gibson, V. C. *Angew. Chem., Int. Ed.* **2006**, *45*, 1241−1244.
(33) Allan, L. E. N.; Shaver, M. P.; White, A. J. P.; Gibson, V. C. *Inorg. Chem.* **2007**, in press.
(34) Shaver, M. P.; Allan, L. E. N.; Gibson, V. C. *Organometallics*, in press, **2007**.
(35) Poli, R. *Angew. Chem., Int. Ed.* **2006**, 45, 5058−5070.
(36) Hsieh, A. T. T.; West, B. O. *J. Organomet. Chem.* **1976**, *112*, 285−296.
(37) Arduengo, A. J., III; Krafczyk, R.; Schmutzler, R.; Craig, H. A.; Goerlich, J. R.; Marshall, W. J.; Unverzagt, M. *Tetrahedron* **1999**, *22*, 14523−14534.
(38) Tom Dieck, H.; Diercks, R. *Angew. Chem., Int. Ed. Engl.* **1983**, *22*, 778−779.
(39) Evans, D. F. *J. Chem. Soc.* **1959**, 2003−2005.
(40) Evans, D. F.; Fazakerley, G. V.; Phillips, R. F. J. *J. Chem. Soc. A* **1971**, 1931−1934.
(41) Grant, D. H. *J. Chem. Educ.* **1995**, *72*, 39−40.
(42) Nielen, M. W. F. *Mass Spectom. Rev.* **1999**, *18*, 309−344.
(43) Dourges, M. A.; Charleux, B. B.; Vairon, J. P.; Blais, J. C.; Bolbach, G.; Tabet, J. C. *Macromolecules* **1999**, *32*, 2495−2502.
(44) Bednarek, M.; Biedroni, T.; Kubisa, P. *Macromol. Chem. Phys.* **2000**, *201*, 58−66.
(45) Stoffelbach, F.; Claverie, J.; Poli, R. *C. R. Acad. Sci. Ser. C* **2002**, *5*, 37−42.
(46) Coca, S.; Matyjaszewski, K. *Macromolecules* **1997**, *30*, 2808−2810.
(47) Matyjaszewski, K.; Wang, J.-L.; Grimaud, T.; Shipp, D. A. *Macromolecules* **1998**, *31*, 1527−1534.
(48) Wang, J.-S.; Matyjaszewski, K. *Macromolecules* **1995**, *28*, 7901−7910.
(49) Peat, I. R.; Reynolds, W. P. *Tetrahedron Lett.* **1972**, *14*, 1359−1362.
(50) Wang, J.-S.; Warin, R.; Jerome, R.; Teyssie, P. *Macromolecules* **1993**, *26*, 5984−5990.
(51) Roos, S. G.; Muller, A. H. E.; Matyjaszewski, K. *Macromolecules* **1999**, *32*, 8331−8335.
(52) Qiu, J.; Matyjaszewski, K. *Macromolecules* **1997**, *30*, 5643−5648.
(53) Shen, Y.; Zhu, S.; Pelton, R. H. *Macromolecules* **2000**, *33*, 5427−5431.
(54) Davies, S. C.; Hughes, D. L.; Leigh, G. L.; Sanders, J. R.; de Souza, G. S. *J. Chem. Soc. Dalton. Trans.* **1997**, 1981−1998.
(55) Calderazzo, F.; Englert, U.; Pampaloni, G.; Vanni, E. *C. R. Acad. Sci. Paris* **1999**, 311−319.
(56) Baker, W. A., Jr.; Lutz, P. M. *Inorg. Chim. Acta* **1976**, *16*, 5−8.
(57) Hermes, A. R.; Girolami, G. S. *Inorg. Chem.* **1988**, *27*, 1775−1781.
(58) Barclay, J. E.; Leigh, G. J.; Houlton, A.; Silver, J. *J. Chem. Soc. Dalton. Trans.* **1988**, 2865−2870.
(59) Chatt, J.; Hayter, R. G. *J. Chem. Soc.* **1961**, 5507−5511.

(60) Matyjaszewski, K. *Curr. Org. Chem.* **2002**, *6*, 67−82.
(61) Matyjaszewski, K.; Woodward, B. E. *Macromolecules* **1998**, *31*, 4718−4723.
(62) Qiu, J.; Matyjaszewski, K.; Thouin, L.; Amatore, C. *Macromol. Chem. Phys.* **2000**, *101*, 1625−1631.
(63) Landini, D.; Rolla, F. *J. Org. Chem.* **1980**, *45*, 3527−3529.
(64) Poshkus, A. C.; Herweh, J. E.; Magnotta, F. A. J. *Org. Chem.* **1963**, *28*, 2766−2769.
(65) Wass, D. F. Ph.D. Thesis, University of London **1999.**
(66) Kliegman, J. M.; Barnes, R. K. *J. Org. Chem.* **1970**, *35*, 3140−3143.
(67) de Kimpe, N.; d'Hondt, L.; Stanoeva, E. *Tetrahedron Lett.* **1991**, *31*, 3879−3882.
(68) Tom Dieck, H.; Svoboda, M.; Greiser, T. *Z. Naturforsch.* **1981**, *36b*, 823−832.
(69) Cloke, F. G. N.; Gibson, V. C.; Green, M. L. H.; Mtetwa, V. S. B.; Prout, K. *J. Chem. Soc. Dalton. Trans.* **1988**, 2227−2229.

MA070756J